

Statistical thermodynamics of membrane bending mediated protein-protein attractions

Tom Chou^{1*}, Ken S. Kim², and George Oster³

¹Mathematics Dept. Stanford University,

²Dept. of Physiology and DAMTP, University of Cambridge

³Dept. of Molecular and Cell Biology, University of California, Berkeley

November 13, 2018

Abstract

Integral membrane proteins deform the surrounding bilayer creating long-ranged forces that influence distant proteins. These forces can be attractive or repulsive, depending on the proteins' shape, height, contact angle with the bilayer, as well as the local membrane curvature. Although interaction energies are not pairwise additive, for sufficiently low protein density, thermodynamic properties depend only upon pair interactions. Here, we compute pair interaction potentials and entropic contributions to the two-dimensional osmotic pressure of a collection of noncircular proteins. In contrast to direct short-ranged interactions such as van der Waal's, hydrophobic, or electrostatic interactions, both local membrane Gaussian curvature and protein ellipticity can induce attractions between two proteins at distances of up to ten times their typical radii. For flat membranes, bending rigidities of $\sim 30k_B T$, and moderate ellipticities, we find thermally averaged attractive interactions of order $\sim 2k_B T$. These interactions may play an important role in the intermediate stages of protein aggregation.

Keywords: aggregation, bilayer, virial, elasticity, plate

1 Introduction

Membrane proteins interact directly via screened electrostatic, van der Waal's, and hydrophobic forces. These are short ranged, operating typically over distances of less than a nanometer. Proteins can also interact indirectly via the bilayer in which they are dissolved. In particular, a protein that is "geometrically mismatched" to the bilayer will induce deformations that affect neighboring proteins. These "solvent induced forces" (the membrane lipids being the solvent) are generated by bending deformations of the bilayer and typically act over many protein diameters.

Membrane associated proteins can aggregate due to bilayer bending mediated interactions. For example, aquaporin AQP1 and CD59 aggregate to tips of pipette-drawn tubules (Cho et al., 1999; Discher & Mohandas, 1996). Previous studies using a continuum approximation for the intervening bilayer membrane, have treated protein-protein interactions and found an r^{-4} repulsion between two identical inclusions (Goulian, Bruinsma & Pincus, 1993; Kim, et al., 1998; Park & Lubensky, 1996;

*Correspondence: Mathematics Dept. 382P, Stanford University, Stanford, CA 94305, email: tc@math.stanford.edu

Dommersnes, Fournier & Galatola, 1998). Goulian *et al.* (Goulian, Bruinsma & Pincus, 1993) also find a weak attractive ($-k_B T/r^4$) interaction arising from Casimir forces resulting from suppressed thermodynamic fluctuations of the intervening membrane. Here, we study in detail a direct mechanical origin for protein-protein attractive interactions. Although bending induced forces between multiple inclusions are not pairwise additive, (Kim, et al., 1998; Kim, et al., 1999), in this paper, we restrict ourselves to low protein densities where only pairwise interactions are relevant. We find that the interplay between protein noncircularity (Kim, et al., 1999) and background Gaussian curvature dramatically affect protein-protein attractions and thermodynamics.

Many membrane proteins are noncircular in the plane of the membrane, including adsorbed polypeptides such as MARCKS (Myat et al. 1997), and bacteriorhodopsin (Luecke et al. 1999), which consists of seven transmembrane helices arranged in an elliptical configuration. Small domains, dimers, or droplets of molecules such as cholesterol or specific lipids can themselves behave effectively as membrane inclusions. Droplets need not be rigid to induce attractive forces among themselves; fluctuations in the droplet shape itself may lead to an effective attraction.

In Section 2 we briefly review the mechanical theory of inclusion-induced bilayer bending (Helfrich, 1973; Kim, et al., 1998; Netz & Pincus, 1995). The lipid membrane is approximated by a thin plate that resists out-of-plane bending. Inclusions such as integral membrane proteins, or surface adsorbed molecules, impose boundary conditions along the contact line between the membrane and the protein. Using elastic plate theory to describe the membrane deformations, we derive the energy for two identical inclusions as a function of their relative position within the membrane surface.

In Section 3, we show that the rotational and translational time scales can be separated, so that we can thermally average out the fast rotational degrees of freedom. The resulting effective potential between two proteins is attractive provided the inclusions are sufficiently non-circular. We use the effective potential to compute the second virial coefficient and show how the attractive interactions affect the two-dimensional protein osmotic pressure. Finally, we discuss biological processes where membrane induced long-ranged protein-protein attractions may play an intermediate role, and propose possible measurements.

2 Membrane inclusions and height deformation

Small membrane deformations (on the scale of the lipid or protein molecules) can be accurately modeled using standard plate theory (Landau & Lifshitz, 1985; Helfrich, 1973)

$$\tilde{E}[H(\mathbf{S}), K(\mathbf{S})] = 2b \oint d\mathbf{S} H^2(\mathbf{S}) + b_g \oint d\mathbf{S} K(\mathbf{S}), \quad (1)$$

where $H(\mathbf{S})$ and $K(\mathbf{S})$ are the local mean and Gaussian curvatures, and b and b_g are their associated elastic moduli. We have assumed a symmetric bilayer and a vanishing spontaneous mean curvature in the absence of the membrane-deforming proteins of interest. For uniform b_g , the Gaussian contribution (the second integral in Eq. 1), when integrated over the entire surface yields a constant that is independent of the relative configurations of the embedded proteins (Kim, et al., 1998; Struik 1994). Thus, the Gaussian energy term can be ignored when considering protein-protein interaction energies.

In an expansion of the free energy about that of a flat interface, $H(\mathbf{S}) \simeq (1/2)\nabla^2 h(x, y)$, where ∇^2 is the two-dimensional, in-plane Laplacian, and $h(x, y)$ is a small, slowly varying height deformation from the flat state (cf. Fig 1). Minimizing $\tilde{E}[h(\mathbf{S})]$ with respect to $h(x, y \in \mathbf{S})$ yields the biharmonic equation

$$\nabla^4 h(x, y) = 2\nabla^2 H(\mathbf{r}) = 0. \quad (2)$$

First consider membrane deformations about an isolated, circularly symmetric inclusion of radius a . If the bilayer midplane contacts¹ the protein perimeter \mathbf{C} (see Fig. 1) at an angle γ , the appropriate solution to Eq. 2 is $h(r) = -\gamma \ln(r/a)$ for $r > a$. We have excluded terms in $h(r)$ of the form $r^2 \ln r, r^2, \text{const.}$ because they are unbounded in energy (Eq. 1), or do not satisfy the contact angle boundary condition at $r = a$. Since $\nabla^2 \ln(r/a) = 2H(r) = 0$ for $r > a$, there is no mean curvature bending energy (proportional to b) residing in the bilayer.

Now consider cases where more than one inclusion are present, or where the contact angles, heights of contact, or the shapes of the membrane associated proteins are noncircular. Three types of noncircularity can arise. The inclusion itself may be noncircular (*e.g.* elliptical), the height of contact of the bilayer midplane to the inclusion may vary along the perimeter \mathbf{C} of the protein, and the contact angle itself may vary along \mathbf{C} . These noncircular boundary effects arise from the detailed microscopic nature of the protein and its interaction with the lipid molecules. When more than one protein is present, the deformations surrounding each protein are not circularly symmetric. A nonvanishing mean curvature, $H(\mathbf{r})$, that gives bounded bending energies can be represented by a multipole expansion,

$$H(r, \theta) = \sum_{n=2}^{\infty} r^{-n} (a_n \cos n\theta + b_n \sin n\theta), \quad (3)$$

where (r, θ) is the radial and angular coordinate about an arbitrary origin. Upon substitution of Eq. 3 into Eq. 1, we find the bending energy $\tilde{E} \sim b \sum_{n=2}^{\infty} (a_n^2 + b_n^2)$. To determine a_n, b_n , we solve $\nabla_{\perp}^2 h(r, \theta) = H(r, \theta)$ and impose boundary conditions (see Appendix A) on $h(r, \theta)$ at \mathbf{C} . In the limit of small noncircularity or low protein concentrations, the largest nondivergent terms are associated with $n = 2$. Wiggly inclusion cross-sections or highly oscillating boundary conditions only weakly affect membrane bending-mediated protein-protein interactions via $n > 2$ terms. We derive the full multibody, interaction energy in Appendix A. The *two-body* interaction energy measured in units of $k_B T$ is

$$E(R, \theta_1, \theta_2; \Delta, K_b, \Omega) = \left| \frac{e^{-2i\Omega}}{R^2} + K_b - \frac{\Delta}{2} e^{-2i\theta_1} \right|^2 + \left| \frac{e^{-2i\Omega}}{R^2} + K_b - \frac{\Delta}{2} e^{-2i\theta_2} \right|^2. \quad (4)$$

The dimensionless separation distance R , protein ellipticity Δ , and background curvature K_b are given by

$$\begin{aligned} R &\equiv \frac{r}{R_0}, \quad R_0 \equiv a\sqrt{\gamma}B^{1/4} \\ \Delta &\equiv \bar{\varepsilon}\sqrt{B} \\ K_b &\equiv a\sqrt{B} \left(\frac{\partial^2 h_b(x_1, x_2)}{\partial x_1^2} \right), \end{aligned} \quad (5)$$

where $B \equiv \pi b/k_B T$ is the dimensionless bending stiffness, and $\bar{\varepsilon} \sim O(\varepsilon)$ quantifies the noncircular nature of each inclusion (see Appendix A). The angle Ω is measured between the line joining the protein centers and the principle axis of curvature defined by the background Gaussian curvature (see Fig. 2). The angles θ_1, θ_2 are measured between the principle axes of proteins 1 and 2 and the same principle axis. The quantity K_b measures the local, externally induced (via other distant proteins or external bending forces) background curvature in this principle axis direction. We show in Appendix A that the dominant effect of distant proteins is to induce mean curvature deformations that decay as $1/r^2$, but

¹The contact angle γ incorporates the details of the molecular interactions between the included/adsorbed protein with the lipid molecules. A molecular dynamics simulation would in principle provide the basis for a quantitative estimate of γ , but is beyond the scope of this paper. We will simply assume that γ is a phenomenological parameter determined by the local chemistry, in complete analogy with the standard liquid-gas-solid contact angle.

constant negative Gaussian curvatures. The local curvature K_b arises only from deformations that are of zero mean curvature. In what follows, our statistical thermodynamic analyses will be applied to the pair interaction energy given by Eq. 4 with the convention $\Delta, K_b \geq 0$.

3 Rotationally averaged interactions

Proteins that are not attached to the cytoskeleton are free to rotate and diffuse within in the membrane. The interaction potential between two membrane-deforming inclusions is a complicated, nonseparable function of their relative major axis angles and separation distance (cf. Eq. 4). Although the energy is a function of the specific separations and angles between two membrane associated proteins, rotational degrees of freedom are sampled faster than the translational of freedom. This can be shown by the following argument.

A small solvent molecule in solution has a rotational correlation time of the order $\tau_{rot} \lesssim 1$ ns, while its translational diffusion constant is $D_{trans} \sim 10^{-6} \text{cm}^2/\text{s}$. Therefore, in the time τ_{rot} it takes for a small solvent molecule to lose rotational correlation, it would have translated

$$\delta r \sim \sqrt{\tau_{rot} D_{trans}} \sim 0.1 \text{nm}. \quad (6)$$

For membrane constituents, such as bilayer lipid molecules, $\tau_{rot} \sim 1 - 5 \text{ns}$, and $D_{trans} \sim 10^{-7} \text{cm}^2/\text{s}$, where τ_{rot} corresponds to rotation about the molecular axis parallel to the normal vector of the membrane (Marsh, 1990). As with small molecules in bulk solution, membrane-bound lipid molecules also move $\delta R \sim 0.1 \text{nm}$ during a rotational correlation time. For larger membrane inclusions such as proteins, both rotation and translational diffusion are slower. If Λ is the relative size of the protein radius with respect to the effective lipid radius, protein rotational correlation times increase by $\sim \Lambda^3$ while D_{trans} decreases with a . Membrane proteins that are not too large, $\Lambda \lesssim 10$ say, diffuse $\delta r \sim 1 \text{nm}$ during the time over which it has lost rotational correlation. Therefore, in the time it takes for a typical inclusion to rotate about its axis, it has diffused less than its own size, typically $\gtrsim 1 \text{nm}$. This estimate is consistent with fluorescence measurements that find $\tau_{rot} \sim 0.1 - 1 \text{ms}$ (Yamada et al. 1999). Rotational time scales for larger proteins may not be much faster than translational motions, therefore, our subsequent model is most appropriate for small, unhindered membrane proteins. We must eventually verify that the protein-protein separation r of interest is greater than the typical diffusion distance δr .

The time scale separation can be implemented by statistically averaging over the principle axis angles of the two inclusions while keeping the distance R and angle Ω between them fixed. Weighting the exact two particle energy over its own Boltzmann weight,

$$E_{eff}(R; \Delta, K_b, \Omega) = Z^{-1} \int_0^{2\pi} E(R; \Delta, K_b \theta_1, \theta_2) e^{-E(R, \theta_1, \theta_2; \Delta, K_b, \Omega)} d\theta_1 d\theta_2, \quad (7)$$

where the rotational partition function

$$Z \equiv \int_0^{2\pi} e^{-E(R, \theta_1, \theta_2; \Delta, K_b, \Omega)} d\theta_1 d\theta_2. \quad (8)$$

Upon substitution of Eq. 4 into Eqs. 7 and 8, and performing the integration (see Appendix B),

$$E_{eff}(R; K_b, \Omega) = \frac{2\xi^2}{\Delta^2} + \frac{\Delta^2}{2} - 2\xi \frac{I_1(\xi)}{I_0(\xi)} \quad (9)$$

where

$$\xi = \Delta \sqrt{\frac{1}{R^4} + \frac{2K_b}{R^2} \cos 2\Omega + K_b^2} \quad (10)$$

The effective interaction potential between two inclusions is defined by the difference between the membrane bending energies of two inclusions separated at distance R and at infinite separation,

$$\begin{aligned} U_{eff}(R; \Delta, K_b, \Omega) &= E_{eff}(R; \Delta, K_b, \Omega) - E_{eff}(\infty) \\ &\equiv \frac{2\xi^2}{\Delta^2} - \frac{2\xi I_1(\xi)}{I_0(\xi)} - \left[2K_b^2 - 2\Delta K_b \frac{I_1(\Delta K_b)}{I_0(\Delta K_b)} \right], \end{aligned} \quad (11)$$

For fixed ellipticity Δ , the set of parameters K_b, Ω and R that gives rise to a minimum at $R^* < \infty$, if it exists, is implicitly determined by

$$\left(\frac{\partial U_{eff}}{\partial R} \right)_{R^*} = 0. \quad (12)$$

For sufficiently small R , $U_{eff} \simeq 2/R^4$, as in the circular protein case.

3.1 Zero background curvature

First consider the case of two isolated proteins embedded in a flat membrane. In the absence of external mechanical forces that impose background membrane deformations, and with other inclusions sufficiently far away, $H_b = K_b = 0$, and $\xi = |\Delta|/R^2$. The effective potential (Eq. 11) becomes

$$U_{eff}(R; \Delta, K_b = 0) = \frac{2}{R^4} - \left(\frac{2\Delta}{R^2} \right) \frac{I_1(\Delta/R^2)}{I_0(\Delta/R^2)}. \quad (13)$$

Without background curvature ($K_b = 0$), there are no defining principle axes, and U_{eff} is independent of how the angle of the segment joining the inclusion centers is aligned. Clearly, an effective attractive interaction can arise for $\Delta/R^2 \gg 1$, when $I_1(\Delta/R^2)/I_0(\Delta/R^2) \sim 1$, and $U_{eff}(R; \Delta, K_b = 0) \sim 1/R^4 - \Delta/R^2$. Although the interaction (Eq. 4) yields both repulsive as well as attractive forces, the Boltzmann thermal average in Eq. 7 favors the lower energy configurations of θ_1, θ_2 . Hence the pair of inclusions spends more time in attractive configurations, resulting in a residual attraction in $U_{eff}(R)$. In the $K_b = 0$ limit, the large R behavior of Eq. 13 is

$$U_{eff}(R) = \frac{2 - \Delta^2}{R^4} + O(R^{-6}). \quad (14)$$

Since the potential becomes repulsive at short distances, an effective ellipticity $\Delta > \Delta^* \equiv \sqrt{2}$ is necessary for the existence of a minimum in $U_{eff}(R)$.

Figure 3a shows the θ -independent effective interaction potential as a function of R for various Δ . As Δ is increased from $\Delta^* = \sqrt{2}$, the minimum radius R^* determined by Eq. 12, decreases rapidly from $R^* \sim \infty$. The $\Delta > \Delta^*$ dependence of R^* is plotted in Figure 3b. Also shown are the corresponding magnitudes of the global minima of $U_{eff}(R; \Delta, K_b = 0)$ as a function of Δ .

Figures 3a,b show that appreciable attractive wells can persist at distances $R \sim 1$. For example, the minimum determined by the set of parameters $\Delta \approx 2$, $R^* \approx 0.9$ and $|U_{eff}(R^*)| \approx 2(k_B T)$ can arise for $\gamma \sim 1$, $\varepsilon/a \sim 0.25$ and $b \simeq 30k_B T$. The separation corresponding to the minimum energy in this case is $r^*/a \simeq 9$, or nine times the inclusion radius. Our initial assumptions using measured and estimated rotational/translational diffusion constants for typical membrane proteins are validated since $\delta r/a \sim 1 - 2 \ll r^*/a$. We conclude that thermally averaged noncircular membrane deformations can induce long-ranged attractive interactions of at least $\sim 2k_B T$ up to distances $\sim 10a$.

3.2 Effect of local Gaussian curvature, $H_b = 0, K_b \neq 0$

A local background curvature may arise due to a nonuniform distribution of distant membrane proteins, or an externally imposed deformation. For example, in the experiments of (Cho et al., 1999; Discher & Mohandas, 1996), a cell is manipulated by a micropipette. A lipid neck is drawn into the pipette and curvature is externally imposed. Regions near the base of the neck will have a large negative Gaussian curvature. Similarly, membrane fusion and fission processes in endo/exocytosis involves intermediate shapes with constricted necks containing Gaussian curvature. These regions may be “externally” imposed by proteins involved in vesiculation (*e.g.* dynamin or motor proteins). The Gaussian curvature in this case may also result from lipid structural or composition changes (Schmidt *et al.*, 1999). Therefore, curvature can couple to membrane protein or lipid shapes.

The Gaussian curvature of the membrane between the two proteins establishes local axes of principle curvature such that $a\partial_{x_1}^2 h(x_1, x_2) = -a\partial_{x_2}^2 h(x_1, x_2) \equiv \eta_b \propto K_b > 0$. Since we assume $H_b = 0$, the background deformation between the two proteins will resemble a saddle with principle curvatures of equal magnitudes (cf. Fig. 2). The rotationally averaged (over θ_1, θ_2) effective interaction $U_{eff}(R; \Delta, K_b, \Omega)$ will generate attractions at specific orientation angles Ω even if $\Delta < \Delta^*$. This can be most easily seen by expanding equation 11 (the rotationally averaged interaction $U_{eff}(R; \Delta, K_b, \Omega)$) in powers of $1/R$ for large R :

$$U_{eff}(R \rightarrow \infty; \Delta, K_b, \Omega) \simeq \frac{A_2}{R^2} \cos 2\Omega + \frac{A_4}{R^4} + O(R^{-6}), \quad (15)$$

where explicit forms for A_2, A_4 are given in Appendix A. The appearance of $A_2 \neq 0$ when $K_b > 0$ immediately generates a minimum, however small. Even when ellipticity vanishes ($\Delta = 0$), $A_2 \propto K_b \cos 2\Omega < 0$ for appropriate Ω .

The physical origin of attractions in the presence of background curvature can be readily seen by considering Figure 2. With our convention $\gamma > 0$, circular proteins situated at low regions of the saddle ($\Omega \sim \pi/2$) develop attractive interactions, while those with $\Omega \sim 0$ always repel. Recall from previous studies that two circular protein repel with a R^{-4} potential (Goulian, Bruinsma & Pincus, 1993; Kim, et al., 1998; Park & Lubensky, 1996; Dommersnes, Fournier & Galatola, 1998). This is a direct consequence of placing a second protein in the Gaussian curvature of the first one. When the background curvature of the membrane in the region between two proteins augments the individual Gaussian curvatures around the first protein (near $\Omega = 0$), the R^{-4} repulsion is also enhanced. Conversely, if the background curvature mitigates the saddle induced by an individual inclusion (near $\Omega = \pi/2$), the other inclusion sees not only a diminished repulsion, but a mutual attraction at large enough distances. This is because the individual Gaussian curvature around a protein (arising from $h(r) \approx -\gamma \ln(r/a)$) decays as $1/r^4$ and eventually becomes smaller than the imposed constant background Gaussian curvature associated with K_b . Attractive effects of the background curvature eventually manifest themselves when $\Omega \sim \pi/2$.

Figure 4a shows the effects of a small amount of local background curvature on the effective interaction potential. For small ellipticity $\Delta \ll \Delta^*$, minima appear for large enough angles Ω (approximately for $\Omega > \pi/4$). For similar background curvatures, but much larger ellipticities, the potential develops a repulsive barrier before becoming attractive for certain Ω . This signals that $A_4 < 0$ for large enough Δ and is depicted in Fig. 4b for $\Delta = 2.5$. In the limit of small K_b , $A_4 < 0$ when

$$\Delta > \Delta^* + \frac{K_b^2}{8} \left(3 + \frac{\sqrt{2}}{2} (3 + \sin^2 2\Omega) \right) + O(K_b^4). \quad (16)$$

There is yet an additional, qualitatively different feature of $U_{eff}(R; \Delta, K_b, \Omega)$ when both Δ and K_b are large. Although typical values of K_b (see Eq. 5) in biological settings is $K_b \ll 1$, we find that large values of K_b and Δ give rise to *double* minima in the interaction potential, especially near $\Omega \simeq \pi/2$.

Figure 4c shows double minima for $\Omega = 7\pi/16, \pi/2$. Additional higher order coefficients such as A_6/R^6 , *etc.* are required to quantitatively describe multiple minima. The two minima are a consequence of the two independent physical effects that prefer energy minima; local Gaussian curvature associated with K_b and effective ellipticity Δ . Typically, the weaker, longer-ranged minimum is predominantly the signature of a large K_b , while the deeper, shorter-ranged minimum (such as that shown in Fig. 3a and 4b) is a feature of ellipticity $\Delta > \Delta^*$. Saddles of order $K_b > 1$ correspond to principle radii of curvature on the order of ~ 10 times the protein size a , and are thus regions of extreme Gaussian deformations. Regions of such warp may would only exist as transient, small systems such as fusion necks. Henceforth, we will restrict ourselves to K_b small enough to only induce one minimum.

Angles Ω which yield attractive interactions can be estimated by considering A_2, A_4 . Assuming $A_4 > 0$, values of $A_2 < 0$ give attractive interactions when $-\pi/4 < \Omega < \pi/4$. When $A_2 > 0$, proteins with orientation $\pi/4 < |\Omega| < 3\pi/4$ will experience attractive forces. However, these conditions are modified if $A_4 < 0$, when some angles within $-\pi/4 < \Omega < \pi/4$ can yield attraction even if $A_2 > 0$. This case corresponds to Fig. 4b where a repulsive barrier at $R > R^*$ arises. A minimum can still arise even at angles where $A_2 \cos 2\Omega > 0$ due to the $-R^{-4}$ behavior. The matching to repulsive behavior at smaller R requires consideration of $+R^{-6}$ terms.

The top panel of Figure 5 shows the radius corresponding to the only minimum of the effective potential U_{eff} as a function of K_b , for $\Delta = 0.5, 2$ and 4 . Both east-west and north-south configurations are shown, with intermediate angles Ω interpolating between the curves. For small ellipticity, the local principle curvature K_b is the predominant source of attraction at larger distances, shown by the thick dashed curve. Increasing K_b destabilizes the effective energy minima near $\Omega = 0$. Above a certain background Gaussian curvature intensity, the effective potential minimum evaporates to $R^* \rightarrow \infty$ for proteins situated at $\Omega = 0$ (solid curves), and the attraction is washed out. For small K_b , the two effects, ellipticity and background Gaussian curvature, complement each other near $\Omega = \pi/2$ in reinforcing an energy minimum. Consistent with Fig. 3a for $\Delta > \sqrt{2}$, R^* in Fig. 5 (thick curves) is smaller for larger Δ . The bottom panel plots the corresponding minimum energies.

The Ω -dependence of R^* and the minimum energy is shown in Figure 6. As expected, for large $\Delta \gg \sqrt{2}$, both R^* and $U_{eff}(R^*, \Omega)$ are fairly insensitive to Ω . When Δ is small, the energy minima and their associated radii R^* , caused predominantly by K_b , are very sensitive to orientation Ω . These behaviors are consistent with the energy profiles shown in Fig. 4b. In fact, for small enough Δ , the minima near $\Omega \approx 0$ are annihilated, independent of K_b . Thus, we see a qualitative difference between attractive potentials generated by intrinsic ellipticity and background Gaussian curvature.

4 The second virial coefficient

We now consider the influence of the effective protein-protein attractions on a low density ensemble of inclusions. By analogy with the molecular origins of the osmotic second virial coefficients of proteins in solution (Neal, Asthagiri & Lenhoff, 1998), we will consider the bending energy contributions to the second virial coefficient for a two-dimensional protein equation of state. The membrane mediated interactions however, are much longer-ranged than those in solution (Neal, Asthagiri & Lenhoff, 1998). Consider the thermodynamic limit and times long enough such that

$$\tau \gg \frac{\ell^2}{D_{trans}} \gg \tau_{rot}, \quad (17)$$

where D_{trans} is the protein translational diffusion constant. On the time scale τ , the inclusions are relatively free to diffuse about the bilayer. They interact among themselves via the rotationally averaged potential U_{eff} that manifests itself on time scales $\gtrsim \tau_{rot}$. For very low protein densities (large protein

separation ℓ), the two dimensional protein osmotic pressure will be nearly that of an ideal gas, analogous to a low density gaseous phase surfactant monolayer at the air water interface. Finite protein size a , and longer-ranged elastically-coupled interactions will give nonideal gas properties. The first correction to ideality in the equation of state is given by the second virial coefficient (McQuarrie, 1976):

$$\frac{\Pi}{k_B T} = \Gamma + B_2 \Gamma^2 + O(B_3 \Gamma^3), \quad (18)$$

where Γ is the surface concentration of protein and B_2 is computed using the formula

$$\begin{aligned} B_2(\Delta, K_b) &\equiv -\frac{1}{2Z} \int_0^{2\pi} \int_0^\infty (e^{-E(R, \theta_1, \theta_2; \Delta, K_b, \Omega) + E_{eff}(\infty)} - 1) R dR d\Omega d\theta_1 d\theta_2 \\ &= -\frac{1}{2} \int_0^{2\pi} \int_0^\infty (e^{-U_{eff}(R; \Delta, K_b, \Omega) + U_\infty(\Delta, K_b)} - 1) R dR d\Omega, \end{aligned} \quad (19)$$

The second virial B_2 represents the small fraction of pairwise interacting proteins. Equations 18 and 19 are nondimensionalized such that the surface density $\Gamma \ll 1$ is measured by the number of proteins in area R_0^2 (see Eq. 5) and the protein osmotic pressure Π is measured in units of $k_B T / R_0^2$. Equation 19 is *exact* and does not require the separation of rotational and translational diffusion times needed for the derivation of $U_{eff}(R; \Delta, K_b, \Omega)$. Here, we do not consider how integrating out the rotational degrees of freedom affect the fixed translational degree of freedom. Instead, we are considering times long enough for equilibration of both degrees of freedom, and their combined contribution to the equation of state via B_2 .

The physical origin and value of K_b used in Eq. 19 is as follows. The local curvature felt by the interacting pair represents an interaction between this pair and some other distant proteins. However, the virial equation of state (Eq. 18) is a systematic expansion in surface density expanded about an ideal, *noninteracting* ensemble. Since membrane bending mediated interactions are not pairwise additive (Kim, et al., 1998), one might be tempted to assume that the presence of other proteins would modify the interaction energy E used in the expression for B_2 . However, these more complicated interactions would depend upon the concentration of the other background proteins, and would generate terms higher order in Γ . In other words, we start at densities so low that the protein ensemble is completely noninteracting. As the density is slightly increased, a pair of protein molecules occasionally interact and perhaps form dimers, with each pair ignorant of any other protein. At this still rather low density, the probability three or more proteins approach each other is negligible. When the density is further increased, one needs to consider the higher order virial terms. Therefore, to second order in Γ , the deviation of the equation of state from ideality is completely determined by the two-body interaction $E(R, \theta_1, \theta_2; \Delta, \bar{K}_b, \Omega)$ and is independent of nonpairwise effects (McQuarrie, 1976). Note however, that the two-body interaction *will* depend on the \bar{K}_b associated with *externally* forced, zero mean curvature membrane deformations. Therefore, for the expansion Eq. 18 to be consistent, the value of $K_b = \bar{K}_b$ to be used in Eq. 19 is that owing solely to external force-generated Gaussian curvatures, independent of the protein density.

Figure 7a shows the numerically computed second virial coefficient as a function of inclusion ellipticity for various \bar{K}_b . As expected for small \bar{K}_b , the virial coefficient becomes increasingly negative as the ellipticity increases. The value for circular inclusions $B_2(\Delta = 0, \bar{K}_b = 0) = \pi^{3/2} / \sqrt{2}$ corresponds to purely repulsive disks with mutual interaction $U(R) = 2/R^4$. At ellipticity $\Delta \simeq 1.69$, $B_2(1.69, \bar{K}_b = 0) \simeq 0$ corresponding to a protein solution that is ideal to second order in surface density. Although when $\Delta \simeq 1.69 > \Delta^* = \sqrt{2}$, U_{eff} has an attractive minimum, its effects are negated by the repulsive R^{-4} part of the interaction such that the overall, effective contribution to B_2 vanishes. For $\Delta > 1.69$, the effective attraction between membrane proteins begins to manifest itself. The second virial is modified

by externally imposed Gaussian curvature. Recall that when $\bar{K}_b \neq 0$, certain angles Ω lead to attractive interactions, even for small $\Delta < \Delta^*$. Since we are now thermodynamically averaging over protein positions and Ω in addition to θ_1, θ_2 , the inclusions will spend more time at attractive, lower energy angles Ω , hence lowering B_2 . Consistent with Fig. 4, larger values of \bar{K}_b for $\Delta > \Delta^*$ lead to stronger repulsions at small Ω , which average into B_2 , making it less negative.

The dependence of B_2 on \bar{K}_b is indicated in Figure 7b. In the absence of ellipticity, B_2 is given by the integral

$$B_2(\Delta = 0; \bar{K}_b) = -\pi \int_0^\infty \left[e^{-2/R^4} I_0(4\bar{K}_b/R^2) - 1 \right] R dR. \quad (20)$$

For $\Delta > 0$, B_2 , found from numerical integration of the full expression Eq. 19, are also shown in Fig. 7b. For $\bar{K}_b = 0$, increasing ellipticity decreases inclusion repulsions and B_2 . As in Fig. 7a, large \bar{K}_b and Δ tend to increase B_2 .

Equation 4 was used in Eq. 19 to compute the curves shown in Figures 7; thus, the protein-protein interaction was assumed to consist of contributions only from membrane bending. The hard core, excluded area of each protein, $\sim \pi a^2$, can be included by modifying $U_{\text{eff}}(R)$ by setting $U_{\text{eff}}(R \leq a/R_0) = \infty$. Although we expect this additional repulsive term to further reduce the effective sampling area of the inclusions, and increase the second virial coefficient, we find that for all reasonable values of R_0 , B_2 does not change noticeably from those shown in Figs. 7. The hard core part of the potential, due to *e.g.* close-ranged van der Waals repulsion, is not statistically sampled by the inclusions since the membrane bending induced interactions ($\sim 1/R^4$) already keeps them far apart.

Since nonpairwise interactions manifest themselves only at third and higher order in Γ , we can estimate their importance by comparing $B_2\Gamma^2$ with $B_3\Gamma^3$. For nonpairwise interactions to be thermodynamically relevant it is necessary but not sufficient that the surface density

$$\Gamma \gtrsim \left| \frac{B_2}{B_3} \right|. \quad (21)$$

Although multibody interactions may be important microscopically, their effects on the low density equation of state, cannot be resolved. Even if the density is high enough for $B_3\Gamma^3$ to be measurable, the value of B_3 is found via a four-dimensional integral over configurations of three membrane proteins. All orientations and distances will be averaged and all components of their interactions, repulsive, attractive, pairwise, and nonpairwise will be included. In other words, one cannot uniquely determine the potential U from a measurement of B_n .

5 Discussion and Conclusions

Proteins beyond the range of screened electrostatic, or van der Waals molecular forces can exert forces on one another by virtue of the deformation they impose on the lipid bilayer. These interactions can be attractive if the proteins have a noncircular cross sectional shape or if the local membrane deformation is saddle shaped (negative Gaussian curvature). For bending rigidities $b \approx 30k_B T$, and protein shape ellipticities $\varepsilon/a \sim 0.25$, we find attractive interactions of a few $k_B T$ acting at a range of ~ 5 protein diameters. Thus proteins of radii $\sim 5\text{nm}$ can interact at distances of $\sim 50\text{ nm}$, much further than any interaction between similar molecules in solution. On a flat membrane ($H_b = K_b = 0$), an effective ellipticity $\bar{\varepsilon} > (2k_B T/\pi b)^{1/2}$ is necessary for a potential minimum to emerge between a pair of proteins.

Although we have presented the model in terms of integral membrane proteins, noncircular peripheral proteins, or lipid/cholesterol/proteins aggregates can also induce local membrane bending. Elastically-coupled interactions between peripheral membrane proteins can mediate dissociation and

binding. Dimerization of noncircular peripheral proteins lowers their absolute energy below that of separated ones, and so they are less likely to dissociate from the membrane. Similarly, in one dimension, adsorbed proteins can bend DNA and affect the binding of a second nearby protein. The effective interactions in that case also depends upon the protein orientation (Diamant & Andelman 1999; Rudnick & Bruinsma, 1999). Moreover, proteins and protein aggregates need not be rigid, as we have assumed here. Noncircular distortions of a lipid or protein domains can fluctuate in such a way as to yield domain-domain interactions of exactly the same form considered here.

Elastically mediated attractions can also manifest themselves in the aggregation of *circular* proteins. Once circular proteins overcome short-ranged repulsions and dimerize, barriers to further aggregation of these elliptical dimers are reduced by dimer-dimer attractions described by Eq. (11). If the inclusions are themselves dimers or higher aggregates that persist on the time scale of rotation, bending mediated attraction would enhance further aggregation.

We have only considered the mechanical energies of the intervening lipid bilayer. However, an ensemble of membrane-bound proteins or a mixture of lipids can manifest itself through other forces. For example, the presence of charged membrane components can induce bending (Chou, Jarić & Siggia, 1997) and initiate endo/exocytosis and organelle trafficking. Protein-protein interactions arising from screened electrostatic forces operate at much shorter distances than those of the bending induced forces. Therefore, by spatially organizing charged membrane components, elastic interactions may also play an indirect role in large scale electrostatically induced membrane deformation.

We also considered an ensemble of surface proteins elastically coupled by membrane deformation and computed the deviation of its equation of state from that of an ideal solute. Although membrane-mediated protein-protein interactions are nonpairwise additive (Kim, et al., 1998), only the two-particle interaction is relevant for sparsely distributed proteins. On a flat membrane the second virial coefficient $B_2 < 0$ when $\bar{\epsilon} \gtrsim 0.95\sqrt{k_B T/b}$ ($\Delta \approx 1.69$). At this ellipticity, the elastically induced $1/r^4$ repulsive interactions just compensate for the rotationally averaged attractions. This dependence on $b/k_B T$ suggests that the cell can regulate protein-protein interactions by varying the lipid composition and hence the bending rigidity of the bilayer. Thus, the formation of cholesterol rafts and lipid domains may have an indirect role in mediating long-ranged surface protein aggregation and activity.

Finally, we propose possible experiments in artificial membrane systems where the surface density can be made small enough for a virial expansion to be valid. Although the two-dimensional osmotic pressure would be difficult to measure accurately, measurements of the association time between dimerized proteins are feasible. Measurements have been made of the lifetimes of gramicidin A channels composed of dimers of barrels in opposite bilayer leaflets as a function of bilayer thickness (Kolb & Bamberg 1977; Elliot et al. 1983). Measurements of dimer lifetimes as a function of lipid tail length may reveal the dependence of the attractive interactions outlined in this paper. In fact, since the second virial coefficient measures the time-averaged fraction of proteins in dimers at low density, their lifetimes are proportional to B_2 for attracting proteins. Moreover, these association lifetimes can be measured in the presence of externally imposed Gaussian deformations. Even though an imposed Gaussian curvature increases the interaction well depth at $\Omega \approx \pi/2$, and destroys the attractions for proteins near $\Omega \approx 0$, the overall statistical effect, is to enhance binding, as is evident from Figures 7. Therefore, we expect that dimer lifetimes can be enhanced for proteins residing in regions of large magnitudes of Gaussian curvature such as the base of extruded tubules. This may be instrumental in recruiting fusagens to the correct location for membrane budding. Dimer lifetimes potentially can be measured by fluorescence transfer of specifically designed hydrophilic moieties attached to membrane proteins. Nonpairwise interactions can only be probed directly by measuring lifetimes and aggregation rates of trimers. This would require statistical analyses of chemical or fluorescence activity among two differently tagged membrane proteins, or single molecule diffusion studies.

We thank J. B. Keller and J. C. Neu for helpful comments and many enlightening discussions. T. C. acknowledges support from the National Science Foundation via grant DMS-9804370. K. K. is supported by a grant from the Wellcome Trust, and G. O. is supported by NSF grant DMS-9220719.

A Interaction energy among noncircular inclusions

We consider the boundary conditions that the height, $h(r, \theta)$, must satisfy and the effects of noncircular proteins on the interaction energies (Kim, et al., 1999). Consider proteins with chemistry that changes the cross-sectional protein shape from circularity by an amount ε . The concomitant changes in lipid contact height and angle are also assumed to be modified by $O(\varepsilon)$. As shown in Fig. 1, the protein perimeter, measured from the protein center is, to order $O(\varepsilon)$,

$$\mathbf{C} \simeq (a + \varepsilon \cos 2(\theta - \theta_i))\mathbf{n}, \quad (22)$$

where \mathbf{n} is the unit normal vector to the curve \mathbf{C} projected onto the bilayer midplane, and $\varepsilon \cos 2(\theta - \theta_i)$ is a small, angle-dependent perturbation measuring the deviation from circularity of protein i . Upon expanding the general boundary conditions $h(\mathbf{C}) = \delta h(\theta)$ and $\mathbf{n} \cdot \nabla h(\mathbf{C}) = -\gamma - \delta\gamma(\theta)$ to lowest order in ε , we arrive at effective boundary conditions:

$$\begin{aligned} h(a) &\simeq \delta h(\theta - \theta_i) + \gamma\varepsilon \cos 2(\theta - \theta_i) + O(\varepsilon^2) \\ \partial_r h(a) &\simeq -\gamma \left(1 + \frac{\varepsilon}{a} \cos 2(\theta - \theta_i)\right) - \delta\gamma(\theta - \theta_i) + O(\varepsilon^2) \end{aligned} \quad (23)$$

where we have for simplicity also assumed the variations $\delta h(\mathbf{C})$ and $\delta\gamma(\mathbf{C})$ to be also of order ε .

In the limit of small noncircularity or low protein concentrations, the dominant nondivergent contribution of $H(\mathbf{r})$ to the energy \tilde{E} is $a_2^2 + b_2^2$. The deformation $h(r, \theta)$ that satisfies $\nabla^2 h(r, \theta) = 2H(r, \theta)$ and Eqs. 23 can be written in the form

$$h(r, \theta) \simeq -\gamma \ln \left(\frac{r}{a}\right) + \sum_{n=2}^{\infty} (f_n(r) \cos n\theta + g_n(r) \sin n\theta), \quad (24)$$

and determine a_2, b_2 . When the proteins have intrinsic noncircularity ($\varepsilon \neq 0$), $a_2^2 + b_2^2$ turns out to be the magnitude of the local Gaussian curvature (since $H_b = 0$), modified by additional θ_i -dependent terms (Kim, et al., 1999). The local Gaussian curvature due to the other j far field proteins, in either case, is calculated using the leading order term $h(\vec{r}) \approx -\gamma \ln |\vec{r} - \vec{r}_j|$, which is simply a superposition of the longest-ranged $\ln r$ terms about each inclusion. The total bending energy $\tilde{E}[H(r, \theta)]$ for an ensemble of N inclusions can be written in the complex form (Kim, et al., 1999),

$$\tilde{E} = \pi b \gamma^2 \sum_j \left| \sum_{i \neq j} \frac{a^2}{(z_i - z_j)^2} - \frac{\bar{\varepsilon}}{2} e^{-2i\theta_j} \right|^2. \quad (25)$$

where $z_i = x_i + iy_i$ is the position of the i^{th} protein in the complex plane, and

$$\bar{\varepsilon} \equiv \left(\frac{\varepsilon}{a}\right) \left(\gamma + 2\frac{\delta h}{a} - \delta\gamma\right) \quad (26)$$

measures the effective ellipticity of the identical proteins. Now consider two relatively isolated, identical proteins $i, j = 1, 2$. The effects of proteins far away are felt via a local Gaussian curvature emanating from these background proteins. Upon explicitly separating these contributions, the pair interaction energy becomes

$$\tilde{E}(r, \theta_1, \theta_2; \eta_b, \Omega) = \pi b \left[\left| \frac{a^2 \gamma e^{-2i\Omega}}{r^2} + \eta_b - \frac{\bar{\varepsilon}}{2} e^{-2i\theta_1} \right|^2 + \left| \frac{a^2 \gamma e^{-2i\Omega}}{r^2} + \eta_b - \frac{\bar{\varepsilon}}{2} e^{-2i\theta_2} \right|^2 \right] \quad (27)$$

where

$$\eta_b \equiv a \frac{\partial^2 h_b(\mathbf{S})}{\partial x_1^2} = -a \frac{\partial^2 h_b(\mathbf{S})}{\partial x_2^2} \quad (28)$$

is the curvature in the \mathbf{x}_1 principle direction due to far-field background inclusions or externally induced deformations $h_b \approx -\gamma \ln |z - z_j|$, $j \geq 3$. The mean curvature expanded about a noncircular protein (Eq. 3) results in a deformation $h(r, \theta)$ with terms proportional to $r^2 \cos 2\theta, r^2 \sin 2\theta$ (Kim, et al., 1998). These term carry zero mean curvature, but constant negative Gaussian curvature. From the expansion Eq. 3, the only mean curvature contribution can be seen to decay as r^{-2} , which we neglect. A further contribution to the local saddle curvature, η_b^2 , felt by the two proteins can arise from externally applied mechanical forces that deform the bilayer in an appropriate way. The angles θ_1, θ_2 are the angles of the principle axes of the inclusion shape (or the height or contact angle functions $\delta h, \delta \gamma$) measured from the principle background curvature axis \mathbf{x}_1 . The angle Ω measures the angle between the principle background curvature axis and the segment joining the centers of the two inclusions. Upon rescaling according to Eq. 5, we arrive at the energy given in Equation 4.

B Rotational averaging

The integrals

$$\int_0^{2\pi} E(R, \theta_1, \theta_2; K_b, \Omega) e^{-E} d\theta_1 d\theta_2 \quad \text{and} \quad Z^{1/2} \equiv \int_0^{2\pi} e^{-E} d\theta_1 d\theta_2 \quad (29)$$

used to compute the rotationally averaged, effective protein-protein interaction involve integration of

$$\int e^{\alpha \cos 2\theta + \beta \sin 2\theta} d\theta \quad \text{and} \quad \int (\alpha \cos 2\theta + \beta \sin 2\theta) e^{\alpha \cos 2\theta + \beta \sin 2\theta} d\theta. \quad (30)$$

The first integral in Eq. 30 can be computed in closed form by substituting the exponents with their Bessel function expansions

$$\begin{aligned} e^{\alpha \cos 2\theta} &= I_0(\alpha) + 2 \sum_{n=1}^{\infty} i^n I_n(\alpha) \cos 2n\theta \\ e^{\beta \sin 2\theta} &= I_0(\beta) + 2 \sum_{n=1}^{\infty} (-1)^n I_{2n}(\beta) \cos 4n\theta - 2 \sum_{n=1}^{\infty} i^{2n+1} I_{2n+1}(\beta) \sin 2(2n+1)\theta \end{aligned} \quad (31)$$

and integrating term by term. The cross-terms of the product of the two equations in Eq. 31 involve single powers of \cos and \sin and vanish upon integration. We are left with

$$Z^{1/2} = 2\pi I_0(\alpha) I_0(\beta) + 4\pi \sum_{n=1}^{\infty} (-1)^n I_{2n}(\alpha) I_{2n}(\beta). \quad (32)$$

An analytic continuation of the sum formula,

$$J_0(\sqrt{\alpha^2 + \beta^2 - 2\alpha\beta \cos \varphi}) = J_0(\alpha) J_0(\beta) + 2 \sum_{n=1}^{\infty} J_n(\alpha) J_n(\beta) \cos n\varphi, \quad (33)$$

at $\varphi = \pi/2$ simplifies Eq. 32 to,

$$Z^{1/2} = 2\pi I_0(\xi), \quad \xi \equiv \sqrt{\alpha^2 + \beta^2}. \quad (34)$$

Finally, the second integral in Eq. 30 can be computed by taking derivatives of $Z^{1/2}$:

$$\int (\alpha \cos 2\theta + \beta \sin 2\theta) e^{\alpha \cos 2\theta + \beta \sin 2\theta} d\theta = \left(\alpha \frac{\partial}{\partial \alpha} + \beta \frac{\partial}{\partial \beta} \right) Z^{1/2}. \quad (35)$$

Using these results, we arrive at the rotationally averaged energy E_{eff} given by Eq. 9. For large separation distances R , the effective interaction $U_{eff}(R) \equiv E_{eff}(R) - E_{eff}(\infty)$ defined in Eq. 11 can be expanded as in Eq. 15 where the coefficients are given by

$$A_2 \equiv 4K_b - 2\Delta^2 K_b \frac{\partial}{\partial \xi} \left(\frac{I_1(\xi)}{I_0(\xi)} \right)_{\Delta K_b} - 2\Delta \frac{I_1(\Delta K_b)}{I_0(\Delta K_b)} \quad (36)$$

and

$$A_4 \equiv 2 - \Delta^2 \frac{\partial}{\partial \xi} \left(\frac{I_1(\xi)}{I_0(\xi)} \right)_{\Delta K_b} - \frac{\Delta}{K_b} \frac{I_1(\Delta K_b)}{I_0(\Delta K_b)} \sin^2 2\Omega - \Delta^2 \left[K_b \frac{\partial^2}{\partial \xi^2} + \frac{\partial}{\partial \xi} \right] \left(\frac{I_1(\xi)}{I_0(\xi)} \right)_{\Delta K_b} \cos^2 2\Omega. \quad (37)$$

References

- Chaikin, P. M. and T. Lubensky. 1995. Principles of Condensed Matter Physics. Cambridge University Press, Cambridge.
- Cho, M. R., D. W. Knowles, B. L. Smith, J. J. Moulds, P. Agre, N. Mohandas, and D. E. Golan. 1999. Membrane dynamics of the water transport protein Aquaporin-1 in intact human red cells. *Biophys. J.* 76:1136-1144.
- Chou, T., M. V. Jarić, and E. D. Siggia. 1997. Electrostatics of lipid bilayer bending. *Biophys. J.* 72:2042-2055.
- Diamant, H. and D. Andelman. 1999. Binding of molecules to DNA and other semiflexible polymers. cond-mat/9910162
- Discher, D. E. and N. Mohandas. 1996. Kinematics of Red Cell Aspiration by Fluorescence-imaged Microdeformation. *Biophys. J.* 71:1680-1694.
- Dommersnes, P. G., J. B. Fournier, and P. Galatola. 1998. Long-range elastic forces between membrane inclusions in spherical vesicles. *Europhys. Lett.* 42:233-238.
- Elliot, J. R., D. Needham, J. P. Dilger, and D. A. Haydon. 1983. The effects of bilayer thickness and tension on gramicidin single-channel lifetime. *Biochim. Biophys. Acta.* 735:95-103.
- Golestanian, R., M. Goulian, & M. Kardar. 1996. Fluctuation-induced interactions between rods on a membrane. *Phys. Rev. E.* 54:6725-6734.
- Goulian, M., R. Bruinsma, and P. Pincus. 1993. Long-range forces in heterogeneous fluid membranes. *Europhys. Lett.* 22:145-150
- Helfrich, W. 1973. Elastic properties of lipid bilayers: theory and possible experiments. *Z. Naturforsch. C.* 28:693-703.
- Kim, K. S., J. Neu, and G. Oster. 1998. Curvature-mediated interactions between membrane proteins. *Biophys. J.* 75:2274-2291.
- Kim, K. S., J. Neu, and G. Oster. 1999. The Effect of Protein Shape on multibody interactions between membrane inclusions. Submitted to Physical Review E.
- Kolb, H. A. and E. Bamberg. 1977. Influence of membrane thickness and ion concentration on the properties of the gramicidin A channel: autocorrelation, spectral power density, relaxation and single-channel studies. *Biochim. Biophys. Acta.* 464:127-141.
- Landau, L. D. and E. M. Lifshitz. 1985. Theory of Elasticity. Pergamon Press, New York.
- Leibler, S. 1986. Curvature instability in membranes. *J. Physique.* 47:507-516.
- Luecke, H., B. Schobert, H. T. Richter, J. P. Cartailler, J. K. Lanyi. 1999. Structure of bacteriorhodopsin at 1.55 angstrom resolution *J. Mol. Bio.* 291:899-911
- McQuarrie, D. A. 1976. Statistical Mechanics. Harper & Row, New York.
- Marsh, D. 1990. CRC Handbook of Lipid Bilayers, (CRC Press, Boca Raton)

- Myat, M. M., S. Anderson, L. A. H. Allen, and A. Aderem. 1997. MARCKS regulates membrane ruffling and cell spreading. *Current Biology*. 7:611-614.
- Neal, B. L., D. Asthagiri, and A. M. Lenhoff. 1998. Molecular Origins of Osmotic Second Virial Coefficients of Proteins. *Biophys. J.*, 75:2469-2477.
- Netz, R. R. and P. Pincus. 1995. Inhomogeneous fluid membranes: segregation, ordering, and effective rigidity. *Physical Review E*. 52:4114-4128.
- Nielsen, C. M. Goulian, and O. S. Andersen. 1998. Energetics of inclusion-induced bilayer deformations. *Biophys. J.*, 74:1966-1983.
- Park, J. M. and T. C. Lubensky. 1996. Interactions between membrane inclusions on fluctuating membranes. *J. Phys. I*, 6:1217-1235.
- Rudnick, J. and R. Bruinsma. 1999. DNA-Protein Cooperative Binding through Variable-Range Elastic Coupling. *Biophys. J.*, 76:1725-1733
- Schmidt, A., M. Wolde, C. Thiele, W. Fest, H. Kratzin, A. V. Podtelejnikov, W. Witke, W. B. Huttner & H-D. Söling. 1999. Endophilin I mediates synaptic vesicle formation by transfer of arachidonate to lysophosphatidic acid. *Nature*, 401:133 - 141.
- Spudich, J. L. 1994. Protein-protein interaction converts a proton pump into a sensory receptor. *Cell*, 79:747-750.
- Struik, D. J. 1961. Lectures on Classical Differential Geometry. Dover, New York.
- Yamada, M., Y. Ohta, T. Sakaki, Y. Yabusaki, H. Ohkawa, & S. Kawato. 1999. Dynamic mobility of genetically expressed fusion protein between cytochrome P4501A1 and NADPH-cytochrome P450 reductase in yeast microsomes. *Biochemistry*, 38:9465-9470.

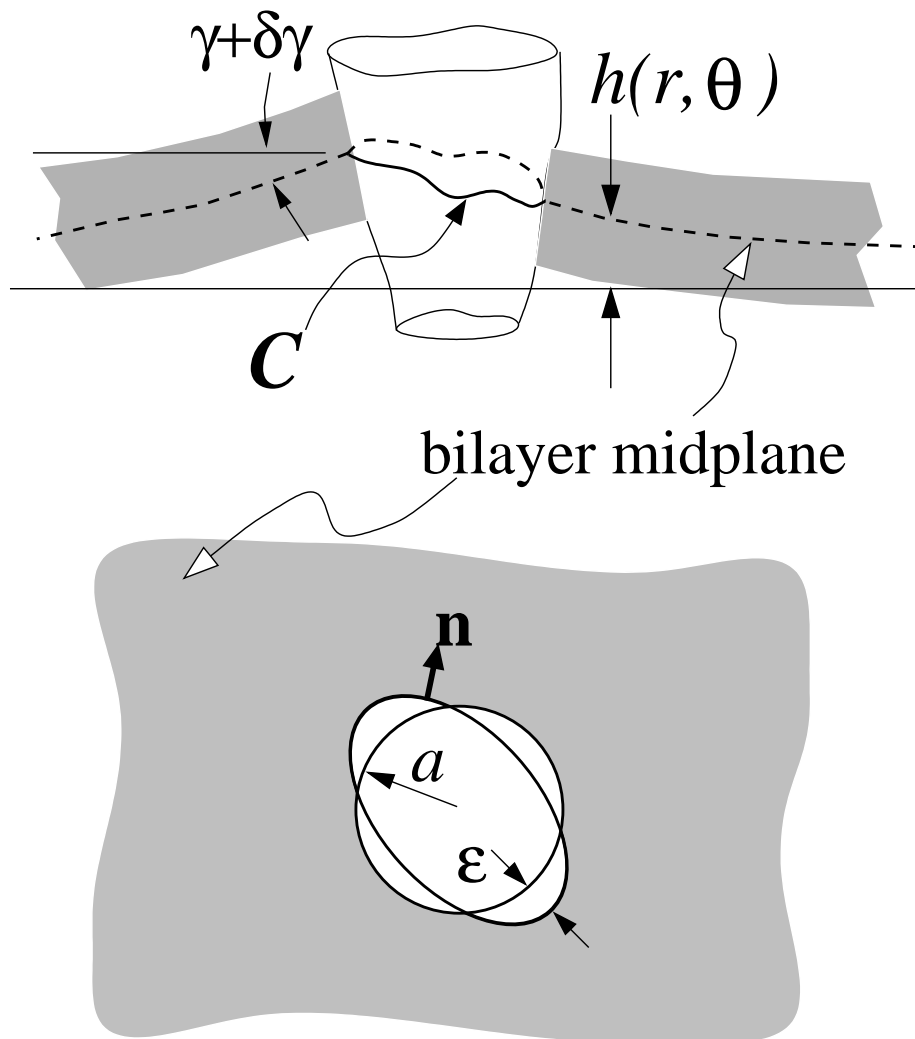


Figure 1: Schematic of a protein inclusion. The top figure is a cut-away view of a membrane protein that contacts the continuum bilayer midplane on curve \mathbf{C} . The contact angle on \mathbf{C} is denoted $\gamma + \delta\gamma$, while the bilayer deviation from a reference flat state is $h(\mathbf{r})$. The bottom picture shows a possible ellipticity ε in the projection of \mathbf{C} onto the midplane.

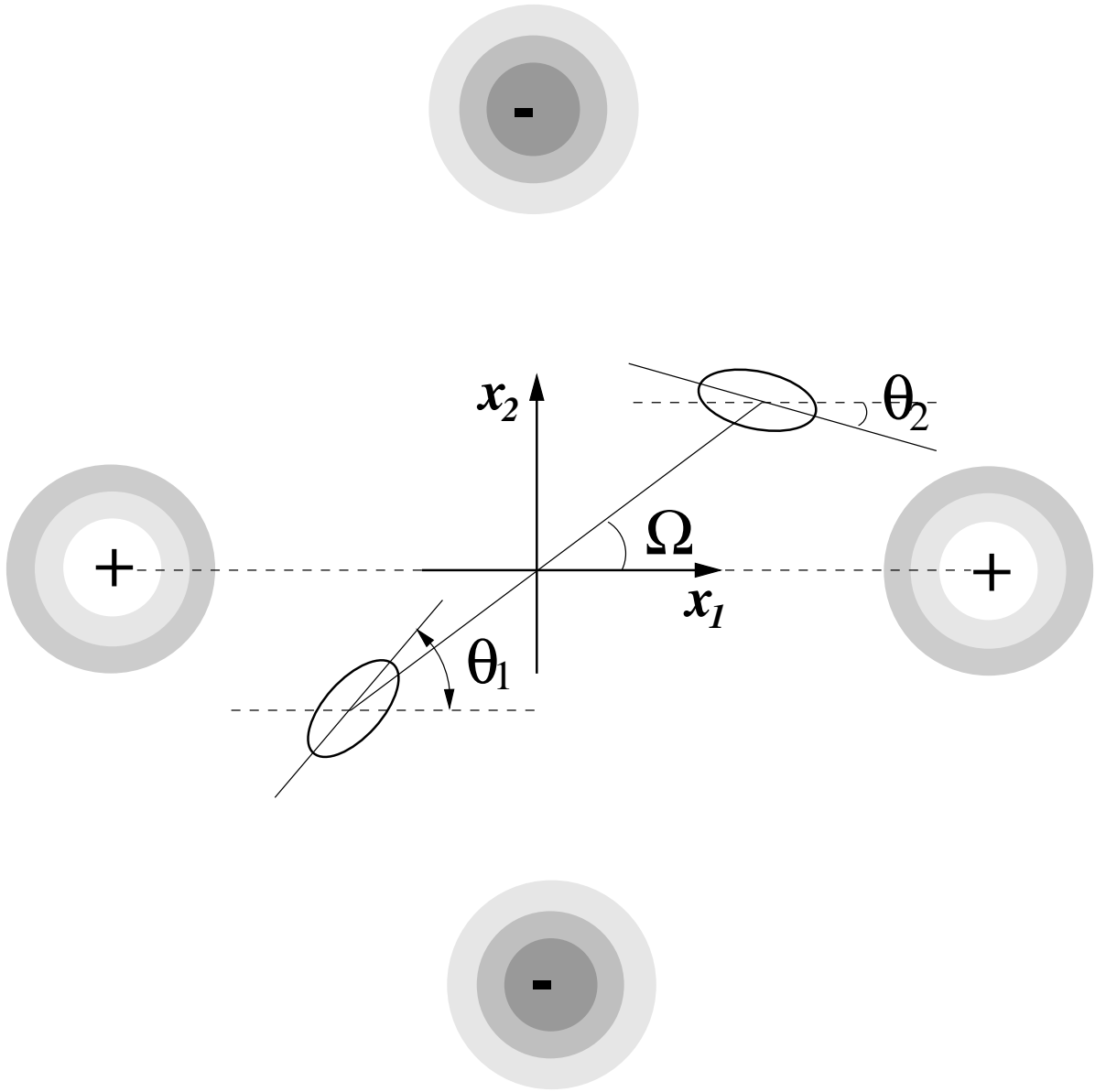


Figure 2: Two inclusions embedded in a local saddle deformation. The $+/-$ correspond to raised/depressed regions of the membrane. The principle axis is aligned with the path joining the two raised regions (east-west). The principle axes of the inclusions (θ_1, θ_2) as well as the centerline joining their centers (Ω) are measured with respect to this principle axis.

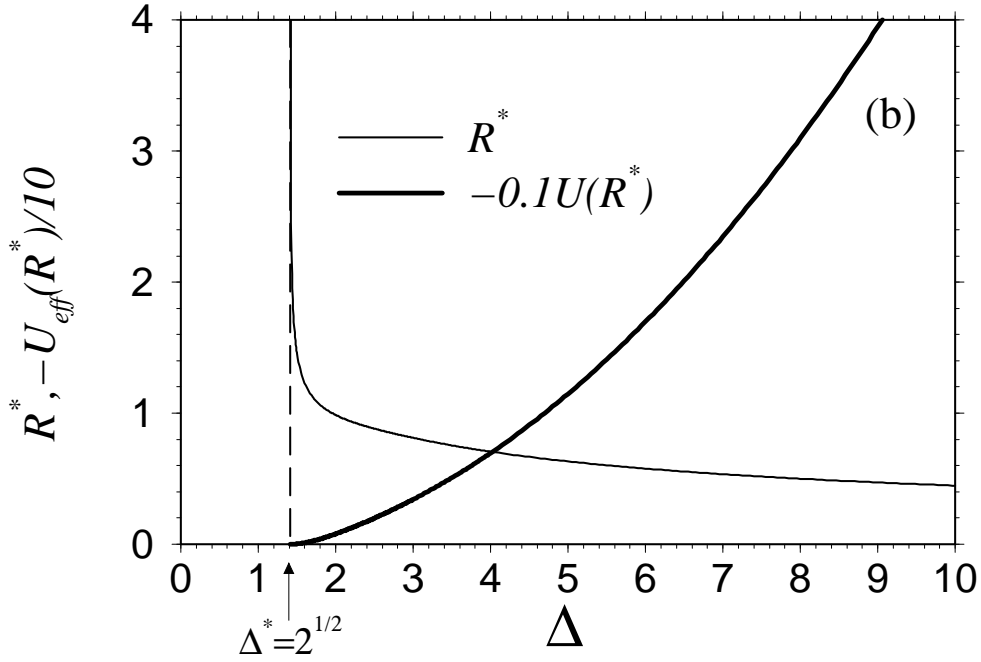
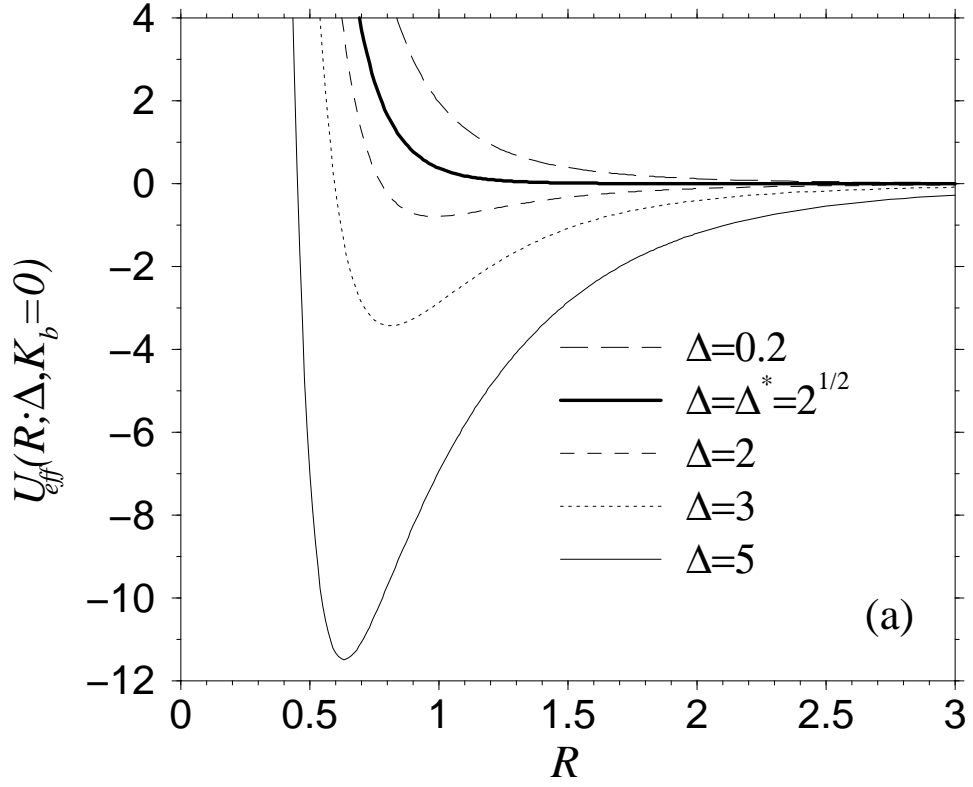


Figure 3: (a). Rotationally averaged effective potential (Eq. 13) as a function of protein separation in a flat membrane ($H_b = K_b = 0$). (b). The minimum effective energy and its associated radius R^* . The minimum of the potential is plotted as $1/10|U_{\text{eff}}(R^*)|$. Note that R^* quickly decreases when Δ increases above $\Delta^* = \sqrt{2}$. For large $\Delta \gg 1$, $R^* \sim \sqrt{2/\Delta}$ and $|U_{\text{eff}}(R^*)| \sim \Delta^2/2$.

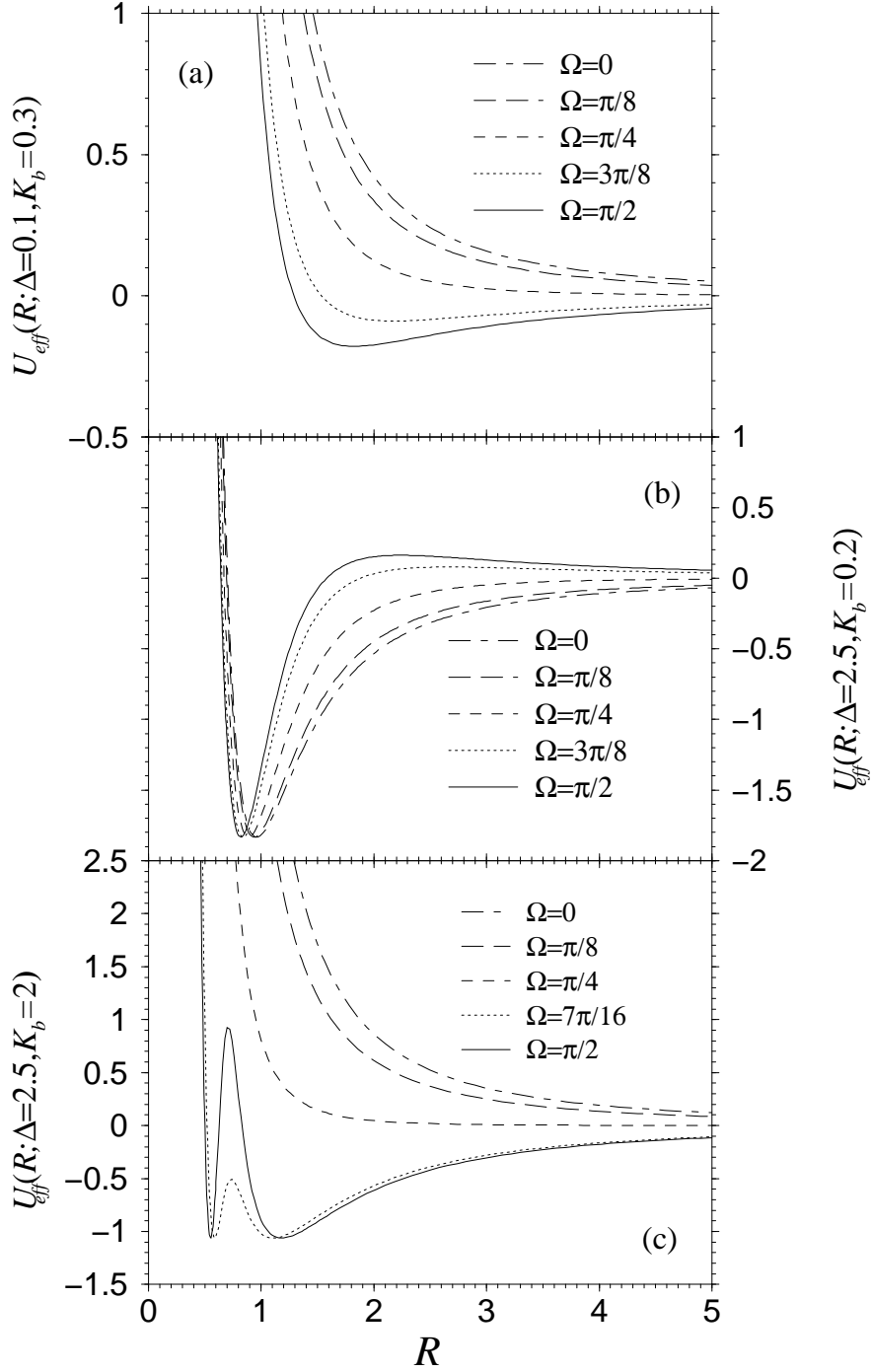


Figure 4: Effective potentials between two inclusions embedded in an $H_b = 0$ and constant K_b membrane. (a). $K_b = 0.3$; $\Delta = 0.1$ for various Ω . (b). $K_b = 0.2$; $\Delta = 2.5$, and (c). $K_b = 2$; $\Delta = 2.5$. This latter case, although rare under physiological conditions, yields two energy minima which are physical manifestations of the qualitatively different minima depicted in (a). and (b).

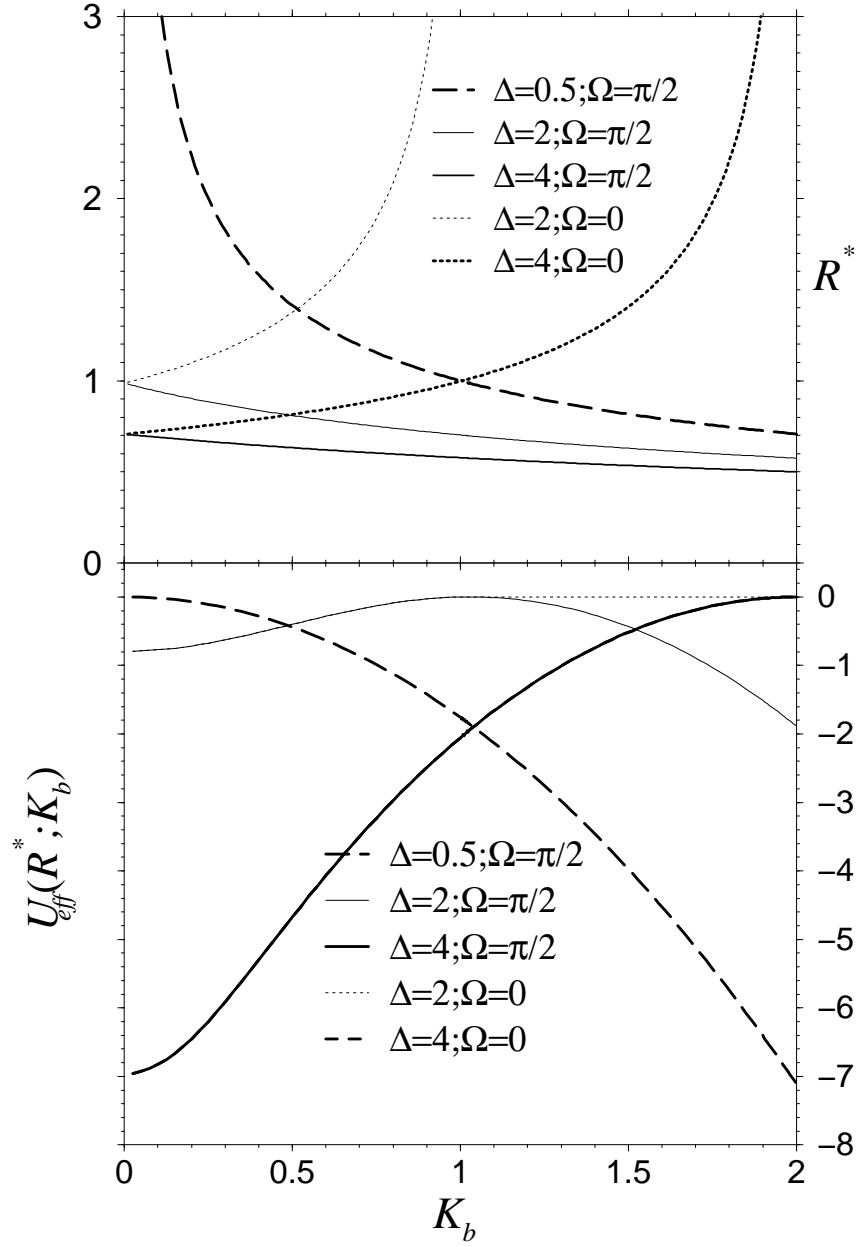


Figure 5: (a). The radii corresponding to interaction potential minima as a function of K_b for $\Delta = 0.5, 2, 4$ and $\Omega = 0, \pi/2$. Curves that diverge signal a loss of the minimum (minimum radius $R^* \rightarrow \infty$) for parameters beyond those indicated. (b). The corresponding potential energy well depths at R^* . The energies associated with $\Delta = 2; \Omega = 0$ and $\Delta = 2; \Omega = \pi/2$ separate at $K_b \approx 1.1$ when the $\Omega = 0$ energy well disappears. The minimum energies associated with large Δ and $\Omega = \pi/2$ is still increasing for $K_b \gtrsim 1.1$.

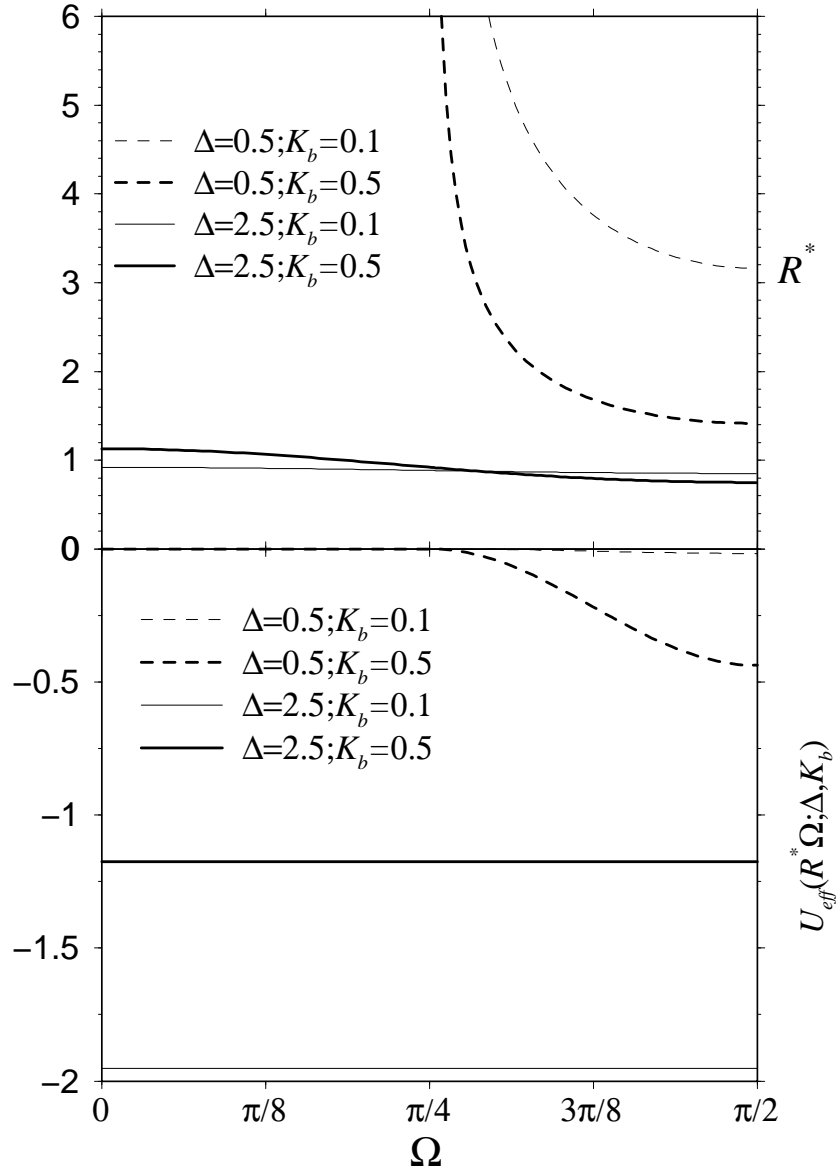


Figure 6: Angular dependence of (a). R^* , and (b). $U_{\text{eff}}(R^*, \Omega)$ as functions of pair orientation angle Ω . Minima arising mainly from background saddle (sensitive to Ω) and ellipticity (insensitive to Ω) are shown.

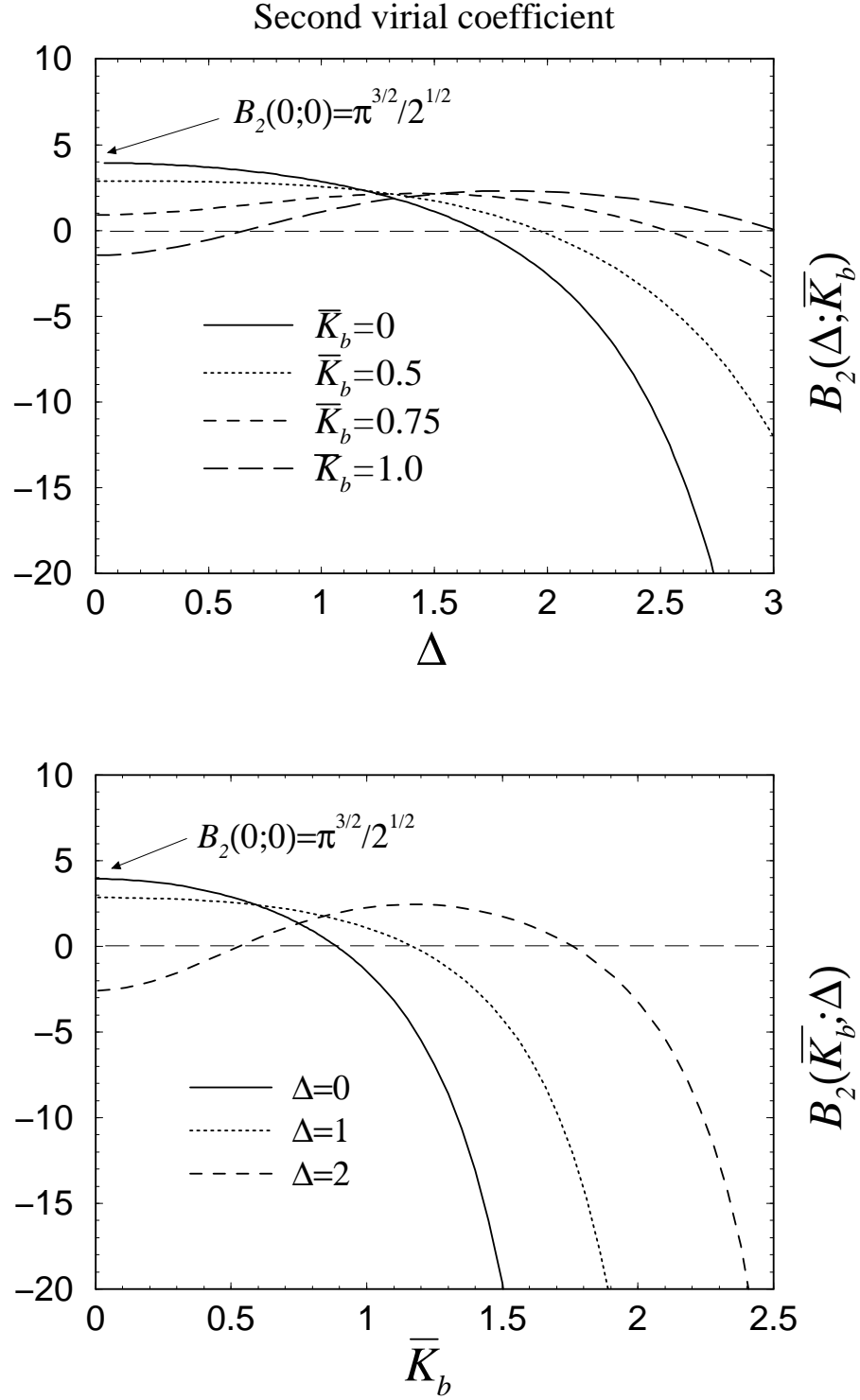


Figure 7: (a). Second virial coefficient $B_2(\Delta, K_b = 0, 0.5, 0.75, 1)$. A negative virial coefficient is indicative of an overall attractive interaction such that the osmotic pressure is *reduced* from that expected in ideal solutions. The value $B_2(0, 0) = \pi^{3/2}/\sqrt{2} > 0$ corresponds to the virial coefficient of circular, repulsive ($U = 2/R^4$) inclusions. (b). B_2 as a function of background saddle for various ellipticity parameters Δ .